Optical fiber sensors implementation for monitoring the early-age behavior of full-scale Timber-Concrete Composite slabs

Mohamed Cheikh Teguedy [a,b,⇑], Catherine Joly-Lapalice [a,c], Luca Sorelli [a,b], David Conciatori [a,b]

[a] Department of Civil and Water Engineering, Laval University, Canada
[b] Research Centre on Concrete Infrastructures-CRIB, Canada
[c] NSERC Industrial Research Chair on Ecoresponsible Wood Construction-CIRCERB, Canada

highlights

- Implementation of DOFs to monitor the short-term behavior of two TCC slabs.
- Monitoring of the strain/temperature during concrete curing.
- Full characterization of the strain evolution along the CLT slabs using DOFs.
- Neutral axis and curvature evolution used to analyse the composite action in TCC.
- Hygrometric variations generated considerable structural changes in TCC at early age.

graphicalabstract

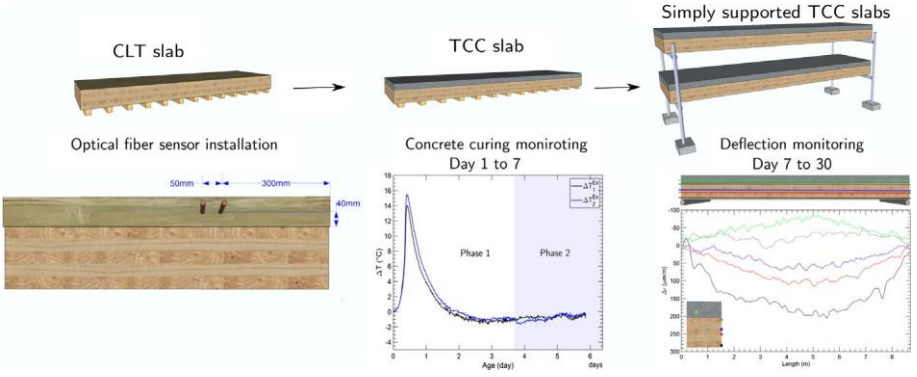

abstract

The study of the early-age behavior of Timber-Concrete Composite (TCC) structures is of great interest as it provides valuable information for manufacturing specification development, quality control, and optimization of the formwork design. In this study, the results of the continuous monitoring of the short-term behavior of TCC slabs using Brillouin Distributed Optical Fiber Sensors (DOFS) are reported. Two TCC slabs with 8.5 m of length were monitored. The composite elements are constituted of Cross-Laminated Timber (CLT) connected to a High-Performance Concrete (HPC) slab. During a monitoring period of about 30 days, the early-age temperature/strain variation in the fresh concrete and in the CLT slab was measured in great details by DOFS. From the presented results, the significant influence of the curing conditions on the early-age shrinkage was highlighted. It was also observed that creep and the daily hygrometric variations of environment affect considerably the composite action between the timber and the concrete. In addition, it was experimentally demonstrated that such mechanisms generate considerable structural changes in the composite elements even before their entry into service.

Keywords:
Timber-Concrete Composite structures
Early-age concrete shrinkage
Hygrothermal deformations
Structural Health Monitoring
Brillouin distributed fiber sensors

1. Introduction

The interest of using timber in contemporary constructions has grown over the last two decades, particularly to design ecological structures with low environmental impact [1]. By connecting timber to concrete it is possible to develop efficient structures in terms

⇑ Corresponding author at: Department of Civil and Water Engineering, Laval University, Canada.
E-mail address: Mohamed-Cheikh.Teguedy@gci.ulaval.ca (M.C. Teguedy).

of strength, stiffness, vibration and acoustic insulation [2–6]. Such structures, called Timber-Concrete Composite (TCC), are promising and viable solutions that can compete, for some applications, with steel and reinforced concrete structures [7].

By making use, in the best way, of advantages of both materials is possible to optimize their structural efficiency and perfor- mances. In a TCC slab, the timber part withstands the tension forces, while the concrete part resists the compression forces and both bears the bending moment. The axial forces engender a com- posite action as an important moment contribution. The connec- tion system allows the transfer of the axial forces as horizontal shear flow at the material interface. There are several challenges to achieve an efficient composite action between both materials, mainly because of the difference in the time-dependent behavior of the timber and the concrete. On one hand, the concrete under- goes, in early-age, complex deformations, i.e. thermal expansion (due to cement hydration heat), creep, drying and autogenous shrinkage, which continue during its entire service life [8,9]. On the other hand, the timber experiences creep and may shrink or swell as a result of the daily hygrometric variations of the environment (''mechano-sorptive'' effect) [10–12]. Consequently, these mechanisms generate internal forces in the composite elements even before their entry into service life [13]. Information about early-age behavior of TCC structures are therefore crucial and must be taken into consideration for the optimization of manufacturing process. For instance, by better knowing the effects of the concrete shrinkage at early-age, it will be possible to optimize the time of the formwork removal or to consider the reduction of the moment resistance due to the initial unknown prestress forces. Note that current practices do not employ a shoring system which can cause an initial deflection due to concrete shrinkage and a possible reduction of the moment resistance due to the self-equilibrated forces induced by the early-age mechanisms [14]. However, despite its importance, little relevant published information is available in the literature concerning the early-age behavior of TCC structures.

In recent years, the emergence of new sensing technologies such as the Optical Fiber Sensors (OFS), offered promising prospects for structural monitoring [15–17]. The versatility, the multiplexing capability, the compact sizes, the lightweight, the relatively low costs and the reliability of such sensors made them very attractive as new options for Structural Health Monitoring (SHM) engineers [18,19]. For the laboratory applications, OFS can also offer an interesting alternative to the traditional sensors, especially for non-standard challenging applications. For investigation at the material scale, researchers generally prefer the use of discrete or quasi-distributed Fiber Bragg Grating sensors (FBG). In this type of sensors, the measured quantity is recorded at a number of fixed, discrete points along a single optical fiber [20]. For large civil engineering structures, Distributed Optical Fiber Sensor (DOFS) are preferred because of their capabilities up to hundreds of kilometers [16].

Today, the principal application of these sensors concerns the monitoring of the existing structures in order to extract relevant information about their performances. However, the future trend in SHM consists of integrating such sensors at the beginning of the construction phase of the structures, in order to gather their whole load history (i.e. including the construction and the pre- service phases) [21–23]. Mostly, the information about the early- age behavior of composite civil engineering structures is of great interest as it permits to bring an immediate awareness about their specific issues, and gives guidance to the experts and the manufac- turers to optimize their construction procedures [24]. In the liter- ature, several studies reporting the applications of FBG sensors regarding the early-age temperature/strain evolution in cementitious materials can be found [25–30]. The OFS offers the possibility to start the monitoring process immediately after the concrete pouring and thus providing a direct method to monitor the curing process and quantify the early-age shrinkage [31,32]. However, to the best of author's knowledge, the tests are performed only at the material scale, as their principal objective was to study the feasibility of embedding the OFS inside the concrete. This study aims at using the Brillouin-based scattering DOFS to observe the complex early-age behavior of TCC structures, which is mainly related to the time-dependent behavior of the timber and the concrete. Two TCC slabs were monitored throughout the first 30 days of their pre-service life. Firstly, the OFS were embedded inside the fresh concrete in order to monitor the strain/tempera- ture development during each stage of its curing process. The effect of the curing conditions on the concrete shrinkage was also investigated. After 7 days, both slabs were simply supported, and the evolution of their deformation was monitored for 23 days using multiple-line DOFS mounted on the CLT part of the slabs. Lastly, the changes of the composite action between timber and concrete was monitored using indicators such as neutral axis position and curvature evolution over the time.

2. Brillouin distributed optical fiber sensors

2.1. Introduction

The OFS can be broadly classified based on the spatial distribution of the measurand into two main categories: distributed sensing and multipoint sensing [20]. A typical OFS system is composed of a standard Optical Fiber (OF) connected to an interrogator. When a light signal is sent through the OF, a part of the signal is reflected to the source (backscattered light) and it is used for sensing purposes. The scattering mechanisms result from the interaction between the light and the medium through which it passes (optical fiber). The analysis of the backscatter allows continuous measurements of the strain and/or the temperature along the entire length of the fiber with a specified sampling interval. Three different scattering phenomena can take place inside the OF, namely the Raman, Brillouin, and Rayleigh scattering. Various technologies are available based on the type of the scattering mechanisms and each one having its own advantages and limitations in terms of the maximum fiber length, the measurement resolution and the spatial resolution. The choice of suitable technology depends on the end-user request and the monitoring solution requirements [20].

In the present study, the Brillouin-based DOFS system has been used. This system can continuously measure the strain and the temperature over large distances (up to 150 km). The operating principles of this system are presented in the following sections with the emphasis on the basic concepts for the users to correctly interpret and asses the measurements provided by these sensors.

2.2. Operating principle

In the Brillouin scattering-based DOFS, the frequency at which the scattered light reaches a peak value is defined as the Brillouin frequency. Each OF is characterized, along its length, by a unique Brillouin scattering pattern, that can be viewed as the ''fingerprint'' of the fiber. A change in temperature or in strain inside the OF results in a shift in the spectrum of light scattered inside it (i.e. the Brillouin scatter signature changes along the fiber). The Bril- louin frequency shift varies linearly (for values of strain and temperature within its tolerance ranges) with the strain change ($\Delta\varepsilon$) and temperature change (ΔT), as given by:

$$\nu_B(T,\epsilon) = C_\epsilon \Delta\epsilon + C_T \Delta T + \nu_B(T_0,\epsilon_0) \quad (1)$$

where C_E is the strain coefficient (MHz/$\mu\varepsilon$), C_T is the temperature coefficient (MHz/°C). ε_0 and T_0 are respectively the reference strain and temperature. The strain and the temperature coefficients depend on the fiber composition, the pump wavelength, the fiber coatings and the jackets [33]. These coefficients are generally pro- vided by the fiber manufacturer. υ_B (T_0; ε_0) is the initial Brillouin frequency along the fiber (the baseline).

It is important to note that in Eq. (1), the frequency shift depends on both the temperature and the strain changes within the fiber. That is, the effect of the strain and the temperature must be separated afterwards from the recorded data [34].

2.3. Strain measurement using DOFS

In the DOFS systems, the measurements are performed at discrete points (sampling points) spaced at a constant interval designated as the ''sampling interval". The measurement at each point is computed as the average over a certain length called ''spatial resolution" [35]. This quantity represents the lowest distance between two independent measurements. Hence, the strain/temperature values at a given sampling point rely on the information contained in the surrounding ones. All the measurements corresponding to a distance smaller than the spatial resolution of the DOFS system are correlated and dependent.

The measurement of the deformation with optical fibers assumes that the strain and/or the temperature experienced by the host material (sample to be tested) is transferred as faithfully as possible to the OF. The OF responds with a shift in Brillouin frequency following the Eq. (1). A typical single mode bare OF is composed of three layers: the fiber core with a diameter of 9 µm covered by the cladding layer with an outer diameter of 125 µm and the external coating. The coating is made of plastics with an outer diameter of 250 µm. Construction sites and the engineering materials present a very aggressive environment for the bare OF to be used and in most cases, which is why it must be protected by an external coating. Thus, several types of cables are available on the market for different applications and referred to as tight buffered cable. However, the presence of the protection in the form of one or several layers may affect the transfer of the strain from the host material to the fiber and causes that only a small portion of the ''real" strain of the host material is sensed [36]. For the applications where large strains need to be measured, it can be reasonably assumed that the fiber follows perfectly the deformation of the host material [37]. However, for the measurement of fresh concrete shrinkage and when a low strain level takes place, the impact of the protective coating of the sensing cable on the strain cannot be neglected. In this case, a bare OF is more suitable, but a strategy must be put in place to protect it during the casting process of the concrete.

2.4. DOFS system used in this study

The DOFS used for the present study is a Brillouin Time Domain Analysis (BOTDA) commercially known as OZ Optics Foresight™DSTS. The configuration of the BOTDA adopted in this study is illustrated in Table 1.

The optical sensor used is a single mode bare OF (SMF-28® Ultra) with 250 µm of diameter. The recommended values for the strain/temperature coefficients were given by the manufacturer [38] and reported in Table 2. The value of the strain coefficient was verified in the laboratory by performing a direct tensile test on the fiber. The strained length of the fiber was about 80 cm. As mentioned above, the strain and the temperature effects were sep- arated by inserting one unbounded fiber inside a loose tube (cop- per tube with 6 mm of diameter) and a second fiber embedded directly in the concrete. For the fibers placed on the CLT, an exter- nal temperature/relative humidity sensor (HOBO MX1101) was used to measure the ambient temperature. The specification of the sensor are given in Table 3.

Table 2
Strain/Temperature coefficients for SMF-28® Ultra optical bare fiber [38].

	C_T (MHz/°C)	C_E (MHz/με)*
Given by the manufacturer	1.0240	0.0529

* Measured at 21 °C.

Table 3
Technical data for the external temperature/ relative humidity sensor (HOBO MX1101).

Temperature Sensor	
Range	−20° to 70 °C
Accuracy	±0:21 °C from 0° to 50 °C
Resolution	0.024 °C at 25 °C
Relative Humidity Sensor	
Range	1% to 95%
Accuracy	±2.5% from 10% to 90%
Resolution	0.05% at 25 °C

3. Experimental set up

Before presenting the experimental set-up, it should be noted that this paper details only the aspects related to the instrumenta- tion and the analysis of the strain/temperature response collected from DOFS system. It is beyond the scope of this study to explore the technical aspect related to the choice of connectors geometry and the structural performances of the TCC slabs. The reason is that both studies were carried out by different research teams.

3.1. Materials properties

Two identical TCC slabs were considered in this study. Their dimensions are reported in Fig. 1. The timber part of the slabs is formed by Cross-Laminated Timber (CLT) consisting of 5 bonded single-layer panels, commercialized under the name Nordic X-Lam 175-5s and were prefabricated and delivered in the laboratory by Nordic. Each layer measures 35 mm in thickness, and the total height of the timber slab was equal to 175 mm (*cf* Fig. 1). The design mechanical properties of CLT, provided by the manufacturer, are reported in Table 4. The concrete used in this study is High-Performance Concrete (HPC) C60, which has been prepared in a central mixing plant and delivered in the laboratory using a truck mixer (*cf* Fig. 3b). For the transport purposes, a retarding admixture MasterLIFE® SRA 20 was added to the concrete. The mixture was fully tested and characterized in the laboratory and its main properties are summarized in Table 4. The concrete slabs were reinforced with a welded mesh constituted of steel bars with

Table 1
BOTDA configuration used in this study.

Sampling Interval	Measurement interval	Spatial Resolution	Frequency Step	No. Averages
0.04 m	20 Min.	0.1 m	3 MHz	40000

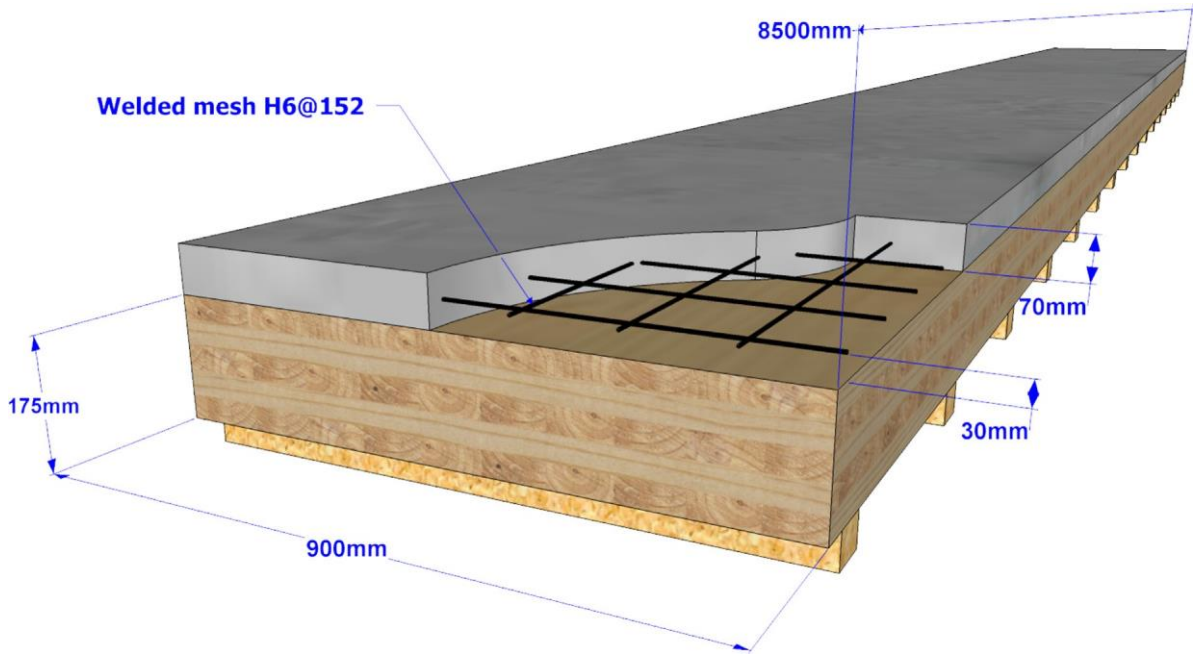

Fig. 1. Schematic illustration of the TCC slab and the shoring system.

6 mm in diameter and designated as MW28 according to standard ASTM A1064 [39]. The reinforcement was placed to resist the tension forces in order to prevent large cracking of the concrete slab. The concrete was cast *in situ* on the top of the timber slabs, and both parts of the TCC slab were interconnected using 8 notch connections spaced by 700 mm. The connection system had a triangular shape and was cut directly in the CLT (*cf* Fig. 2) [40]. The connections were reinforced with steel screws (8 mm x 180 mm), embedded at length of about 155 mm.

The TCC slabs were cast on 15 supports uniformly spaced and were kept on them for the first 7 days. A plastic film was laid over the slabs directly after the casting to ensure wet curing of the concrete. After 7 days of curing, both slabs were simply supported (*cf* Fig. 3c). They were then conditioned 23 days in the laboratory under a controlled temperature at 21 °C ± 0.5 °C, while the relative humidity was not controlled.

3.2. Sensors arrangement and monitoring program

The instrumentation and the monitoring of the slabs using DOFS system evolved during the different phases of the manufac- turing process. This is illustrated graphically in Fig. 4 and detailed in the following paragraphs:

- Phase 0: The BOTDA interrogator requires access to both ends of the fiber. Hence, the OFS were installed inside the concrete formwork in two loops, with a single loop for each of the slabs. A loop is subdivided into two paths: the first one is directly in contact with the concrete and sensitive to both strain and temperature, while the second one is mechanically isolated and sensitive only to the temperature. By combining the measurements from both paths in the same loop and assuming that both paths undergo the same temperature, a separation of the temperature and the strain is then possible in the Eq. 1.
  This was practically achieved by installing the fiber in solid jackets (6 mm copper tube) that cross the slab along its length. The ends of the tubes pass through holes in the transverse wall of the formwork (*cf* Fig. 5). They protect the OF during the concrete casting process and as copper is an excellent heat conductor it ensures a faithful transfer of the temperature from the concrete to the OF. After the casting, one of the gains was carefully slid through the end of the formwork leaving the fiber in direct contact with the concrete. The fluid concrete is prone to shrinkage, coats perfectly the fiber. The tube in the second part of the loop is left embedded inside the concrete throughout the test.
- Phase 1: In this phase, the curing process of concrete slabs was monitored for 4 days. The sensor inside the slabs measured the temperature/strain changes with respect to a reference state defined by a baseline. The optical sensor signal was set to the baseline after one hour from the casting of the concrete. The evolution of temperature/strain was continuously recorded with a measurement time interval of 20 min. During this phase, both slabs were placed on several shoring supports and were maintained under wet curing using the plastic sheeting method (specified by the standard ACI 308R-16ACI [41]). The concrete surface was maintained continuously wet under the plastic sheet during the curing period.
- Phase 2: In this phase, the effect of curing condition on the shrinkage of concrete is investigated. For this purpose, the slab#1 was maintained under the wet curing and the slab#2 was exposed to air (*cf* Fig. 4). It should be noted that before proceeding to the dry curing of the slab#2, it was experimentally verified that the concrete has reached at least 70% of the specified 28 days strength (see Table 4), as specified by [41].
- Phase 2A: In this phase, both slabs were disconnected from the FO system before being placed the simple supports. At the same moment, four lines of fibers were installed at different height on the timber as shown in Fig. 6. Note that the fibers were glued along the CLT layers that are oriented in the longitudinal direction. Then the new loop was connected to the already existing loop inside the concrete. At the beginning, both slabs were equipped with OF sensors. However, as for the Phase 3, the FO sensors of the slab#2 were damaged by the moving operation of the slab and it was then decided to equip the slab#2 with a displacement transducer to measure its deflection at the center. For the fibers installed on the timber, the temperature compen-

Table 4
Materials properties.

Material properties	Measure	Standard
Fresh Concrete		
Water-cement ratio	0.31	–
Air content	1.8%	ASTM C231-17a
Slump (mm)	220 mm	ASTM C143
Temperature	22.5 °C	–
Hardened Concrete		
Compressive strength (1 day)	30.8 MPa	ASTM C39-18
Compressive strength (4 days)	44.7 MPa	ASTM C39-18
Compressive strength (28 days)	63.6 MPa	ASTM C39-18
Tensile strength (28 days)	4 MPa	ASTM C496-17
Elastic modulus (4 days)	24.8 GPa	ASTM C469-14
Elastic modulus (28 days)	30.0 GPa	ASTM C469-14
Shrinkage strain (56 days)	330 $\mu m/m$	ASTM C157
Design properties of CLT slab[a,b]		
Bending Stiffness (EI)	4140 (10^9 N-mm^2/m)	–
Bending moment resistance	87 (10^9N-mm^2/m)	–

[a] Design properties according to the manufacturer.
[b] Properties of the slab according to major strength direction.

sation was achieved using an external temperature sensor. For the fiber embedded inside the concrete, the compensation was done following the same procedure used in the previous phases.

- Phase 3: In this phase, the evolution of the deformation of the simply supported slabs was monitored from the days 7 to 30. During this period, both slabs were only subjected to the uniformly distributed loads resulting from their self-weight (~2.28 kN/m) and the concrete shrinkage. The OFS were set to the baseline when the slab was still on the ground. This way, the strain due to the self-weight of the slab was directly logged in the measurements. After four days from the beginning of this phase, the fiber embedded inside the concrete part of the slab#1 was damaged and was removed from the loop. The monitoring of the timber was continued using the same baseline.

4. Monitoring results and discussion

In the following sections, the monitoring results recorded by DOFS during the first 30 days of the slabs life are presented and

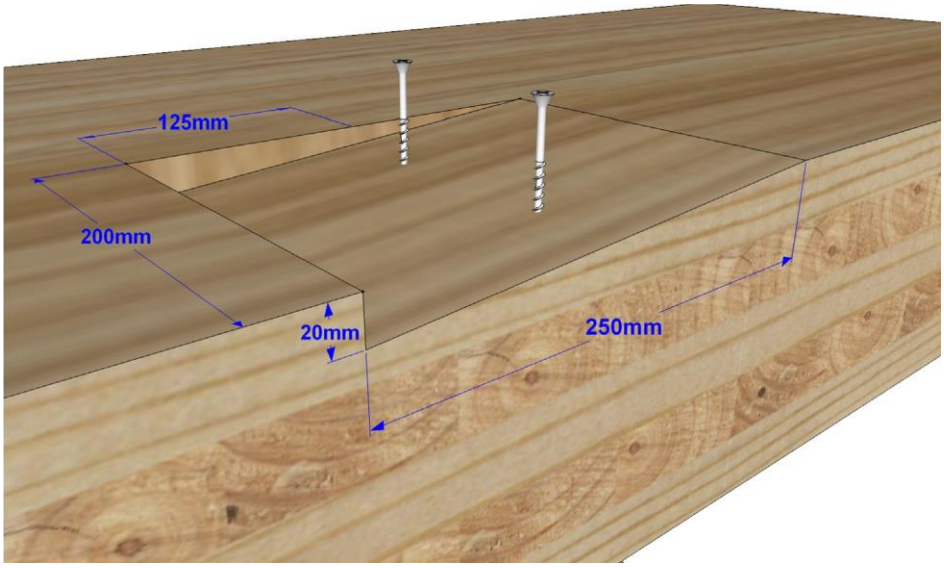

Fig. 2. Details of the triangular notched connection system.

Fig. 3. Fabrication procedure of the TCC slabs. (a) view of CLT-slabs before the concrete pouring, (b) TCC slabs after the concrete casting and (c) slabs placed being simply supported.

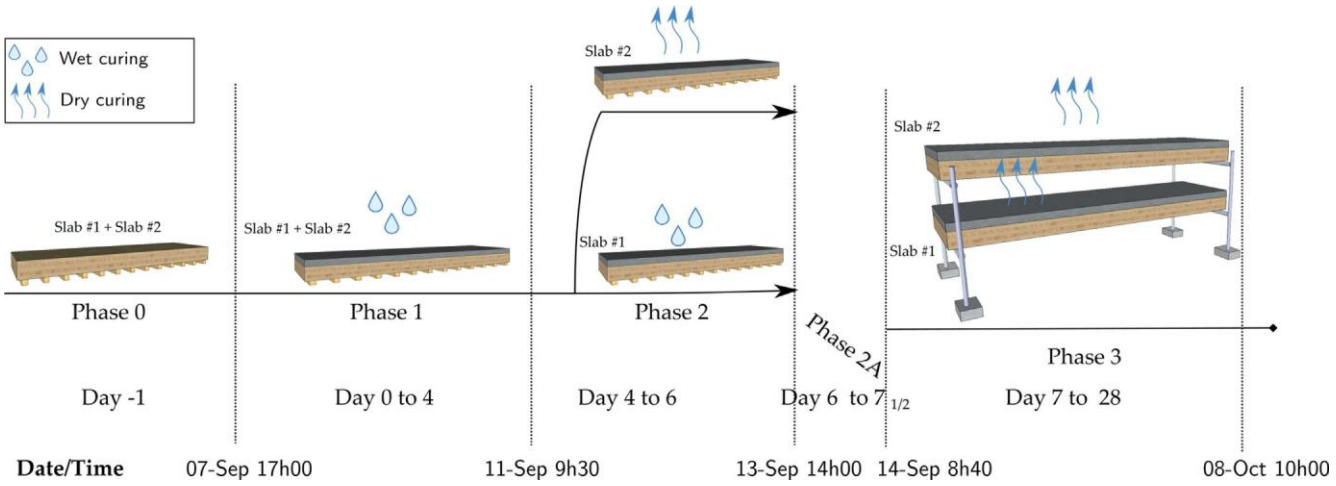

Fig. 4. Summary of construction and monitoring periods of the TCC slabs.

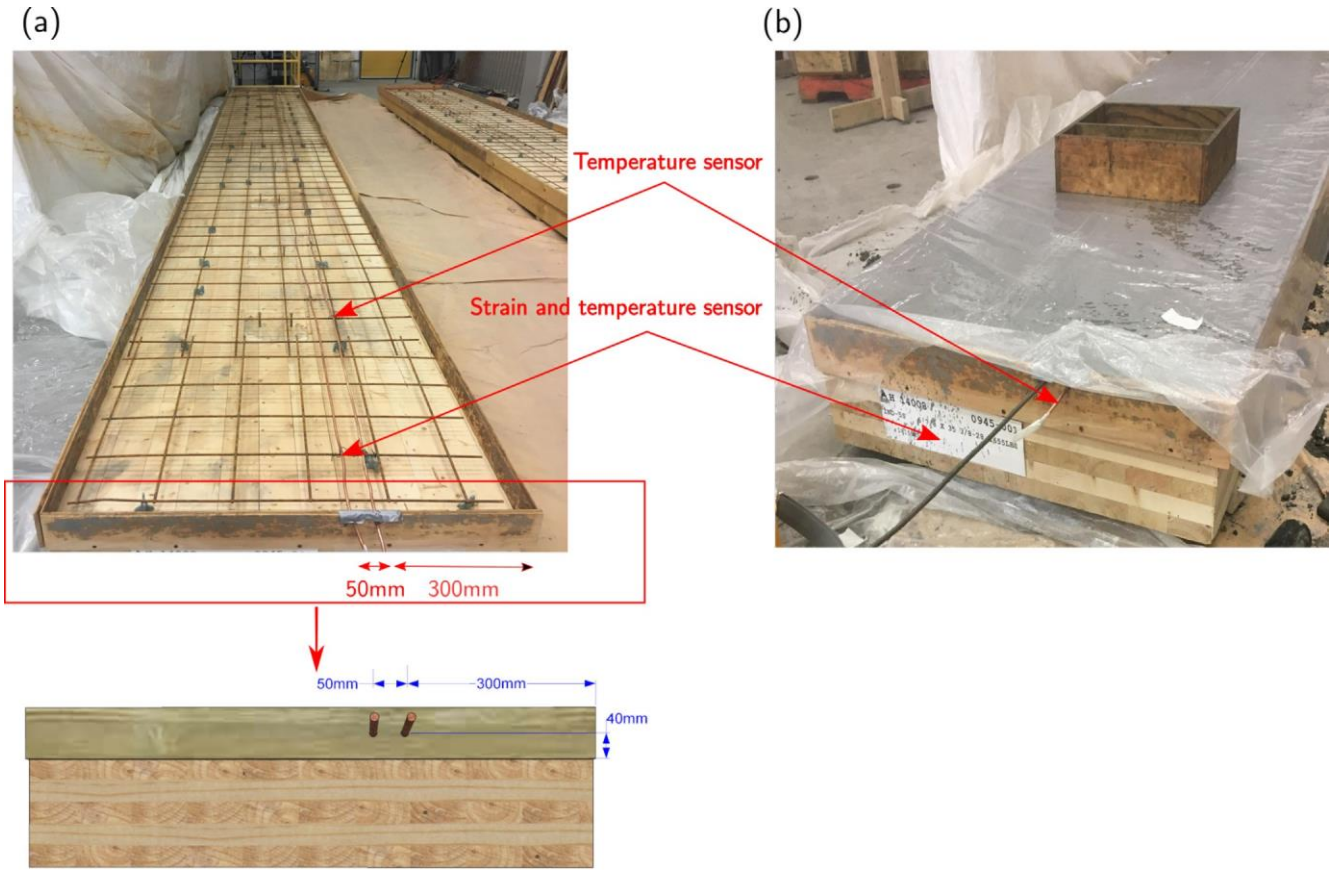

Fig. 5. (a) Cooper tube are positioned inside the formwork in order to encapsulate the fiber during the concrete casting; (b) process of removing the tube once the concrete has been poured leaving the fiber directly embedded inside the concrete slab.

discussed. The results are introduced chronologically according to the monitoring program presented in Section 3.2.

4.1. Concrete curing

4.1.1. Data Processing: temperature compensation

The temperature and the deformation in the concrete part of both slabs were monitored for 6 days. As explained in Section 2.2, the changes in fiber's temperature and/or deformation generate a shift $\Delta\nu$ in the Brillouin frequency. This quantity represents a linear combination of strain and temperature changes inside the mate- rial, as expressed in Eq. 1. The temporal evolution of $\Delta\nu$ in MHz along the length of the fiber is illustrated in Fig. 7. This representa- tion is quite useful because it gives an overall view of the temper- ature/strain evolution in the slabs.

Along each loop, two paths (waves) can be distinguished: the first one corresponds to the temperature sensor (designated here as T*i*, with i being the slab number). The second one corresponds to the fiber that is in contact directly with the concrete (ε-ΔT sensor designated as ST*i*). It can be observed that there is a clear

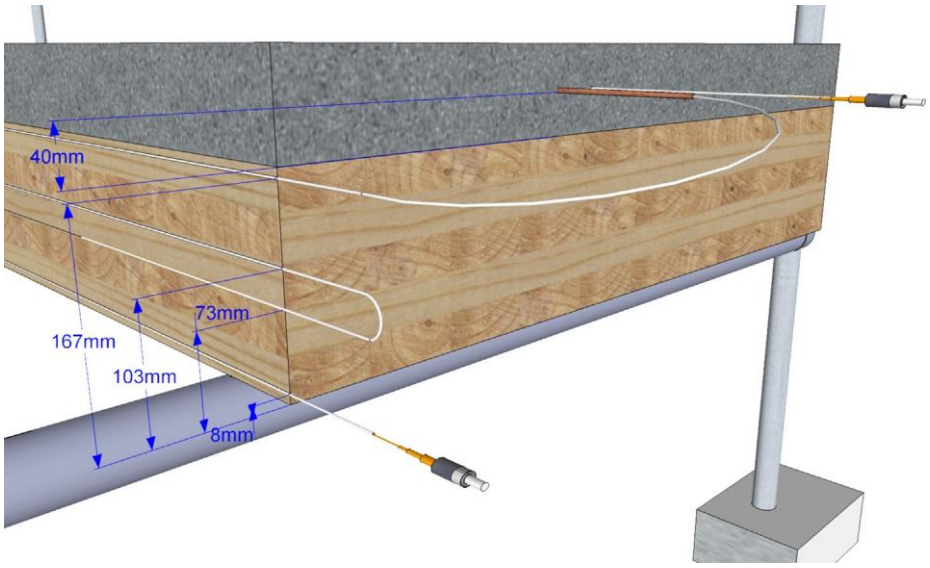

Fig. 6. Fiber arrangement for the slab monitoring during the phases 2A and 3 (*cf* Fig. 1). The primary fiber loop that was embedded in the concrete during the Phase 1 was extended to the timber part of the slab.

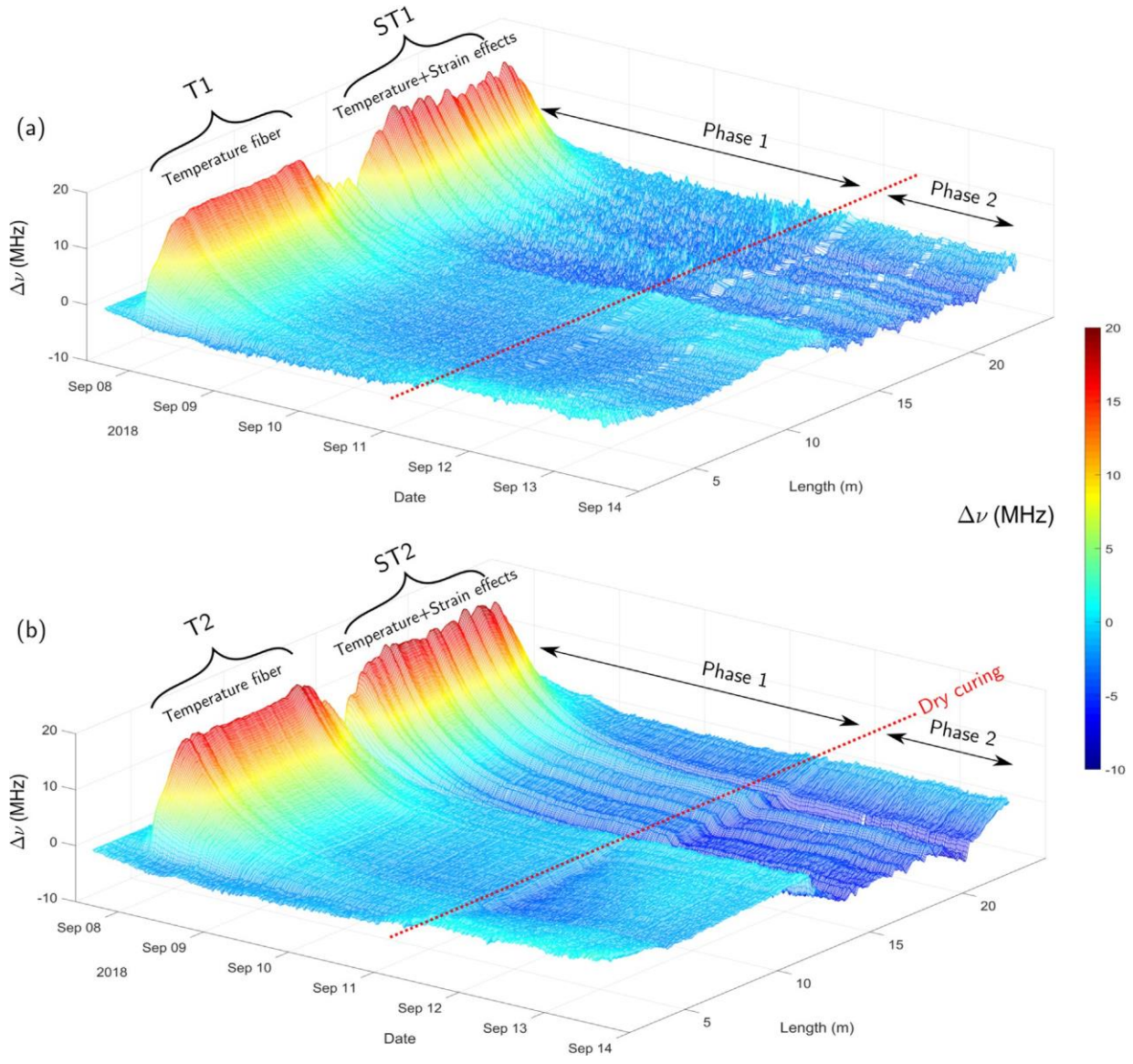

Fig. 7. Temporal evolution of Brillouin frequency shift along the fibers placed inside concrete slabs during the curing process. (a) slab#1 and (b) slab#2.

difference between the T*i* and the ST*i* curves because of the different embedment conditions of the sensors. As a general observation, the fiber inside the concrete (ST*i*) shows larger fluctuations in frequency measurements compared to the one placed in the cooper tube (T*i*). During the Phase 1, both slabs exhibit similar quantita- tive behavior indicating good repeatability of the measurements.

The effect of the hydration heat released by the curing process of the concrete can be observed on the curves as it indices an increase in the frequency shift. The maximum value of the Brillouin frequency shift was reached after about 10 h from the concrete casting. It then gradually decreased to the reference frequency and then essentially remained constant.

From these curves, it is possible to obtain the strain and the temperature changes inside the concrete with Eq. 1. To do so, this equation must be solved at each point along the fiber length. In this case, the signal relative to the temperature (T*i*) and the one representing both the strain and the temperature (ST*i*) must be perfectly aligned. The spatial resolution of the sensing system is about 10 cm which makes it difficult to associate precisely the measured data along the fiber with its position on the slab. A practical solution proposed here is to align the fiber using the cross-correlation product, which measures the similarity between T*i* and shifted (lagged) copies of ST*i*. As the effect of temperature is sensed simultaneously by both signals (T*i* and ST*i*), they show some similar features and thus can be precisely aligned. An example of such procedure is illustrated in Fig. 8. Δυ along the sensors T1 and ST1 after 10 h of the beginning of the test is represented in Fig. 8a. As the fiber was arranged in a loop, the ST1 signal has been inverted to have the same orientation as T1. The shift corresponding to the higher cross-correlation coefficient (0.16 m in this case) was used to align both signal Fig. 8b and c. After the correction of the Brillouin frequency shifts for misalignment issue, the temperature and strain can be retrieved.

4.1.2. Temperature and strain evolution in the concrete

Fig. 9 illustrates the temperature and the strain evolution in the concrete during Phases 1 and 2. The recording of the temperature and relative humidity of the environment during these phases is also presented in Fig. 10. During the wet curing phase (Phase 1), both slabs experienced almost identical behavior. The heat due to the hydration process of the concrete generated a strong increase in the temperature along the length of the slabs. The temperature increased rapidly to reach a peak after about 10 h from the time of concrete pouring (*cf* Fig. 9a and c). It then decreased gradually and cooled down to a steady state. Some slight differences exist in the deformation of both slabs during the Phase 1.

Indicatively, the difference is about 40 μm/m in the length range in between 6 and 8 m. This difference for such portion of the slab is less than 20% of the deformation range measured and it is reasonable for heterogeneous materials such as the fresh concrete. Although the DOFS provide only the measurement of temperature changes, knowledge about the concrete temperature at the beginning of the monitoring (about 22.5 °C) was useful to have an estimate of the absolute value of the temperature. The maximum temperature change in the concrete is about ΔT = 18 °C, which corresponds to an internal absolute temperature in the concrete of 41°C.

Fig. 9a and d show the evolution of the strain along the length of both slabs. At the very early-age (first 24 h), both slabs underwent thermal expansion as results of the heat generated from the cement hydration reaction. Thus, expansion and temperature were observed to reach peak values at the same time. After the initial expansion, the concrete began to shrink monotonically. It should be noted that such observations are in concordance with those generally observed in the literature for cementitious materials [30,42,43]. In addition, the distribution of the strain along the

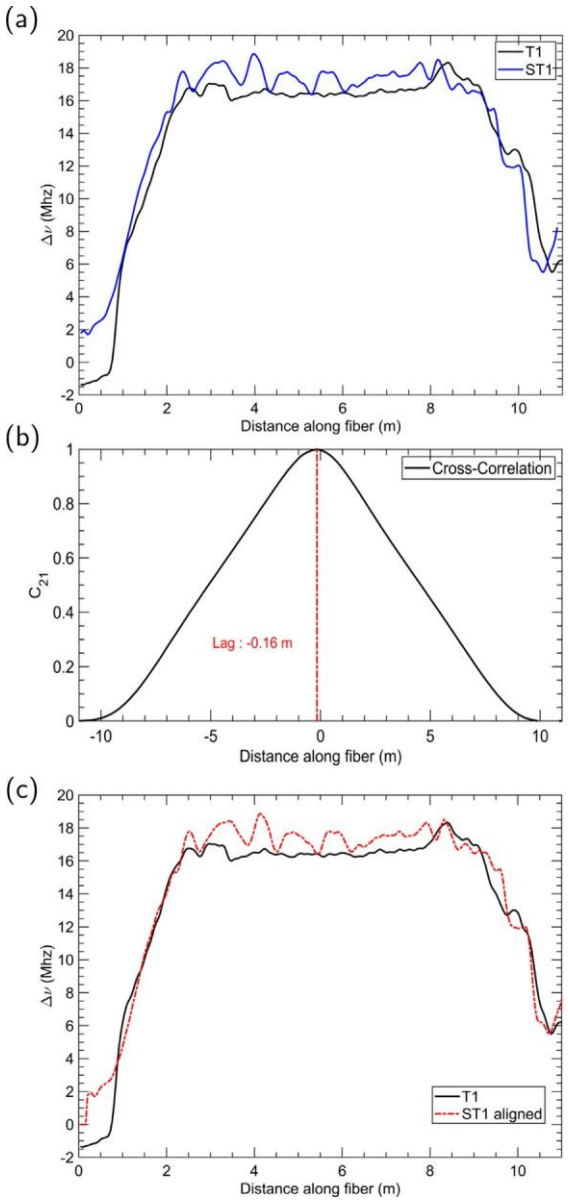

Fig. 8. Illustration of procedure for the fiber alignment. (a) T1 and ST1 signals before alignment, (b) normalized cross-correlation coefficient of T1 and ST1 and (c) alignment of ST1 with respect to T1.

length of the slab seems heterogeneous, especially during the Phase 2, when slab#2 was exposed to air (*cf* Fig. 9d). The highest contraction seems to occur at the extremities of the slabs which may be the indication of possible curling effect. This effect results from the moisture gradient and the temperature differential across the slab thickness [44].

This behavior can be better visualized in Fig. 11, where the evolution of temperature and deformation changes at the center ($\Delta\varepsilon^{Cen}$; ΔT^{Cen}) and at the extremity ($\Delta\varepsilon_i^{Ex}$; εT_i^{Ex}) of both slabs are

illustrated. The position of the considered sections is indicated by dashed lines in Fig. 9. It was clear from these curves that the deformation at the extremities of the two slabs was more pronounced than that at the center. For the temperature, the difference between the extremity and the center was not significant. At the end of the Phase 1, the temperature change was slightly negative. This suggests that the temperature of the concrete was 2 °C higher than the ambient temperature of the room (21 °C) when the baseline for the OFS was set.

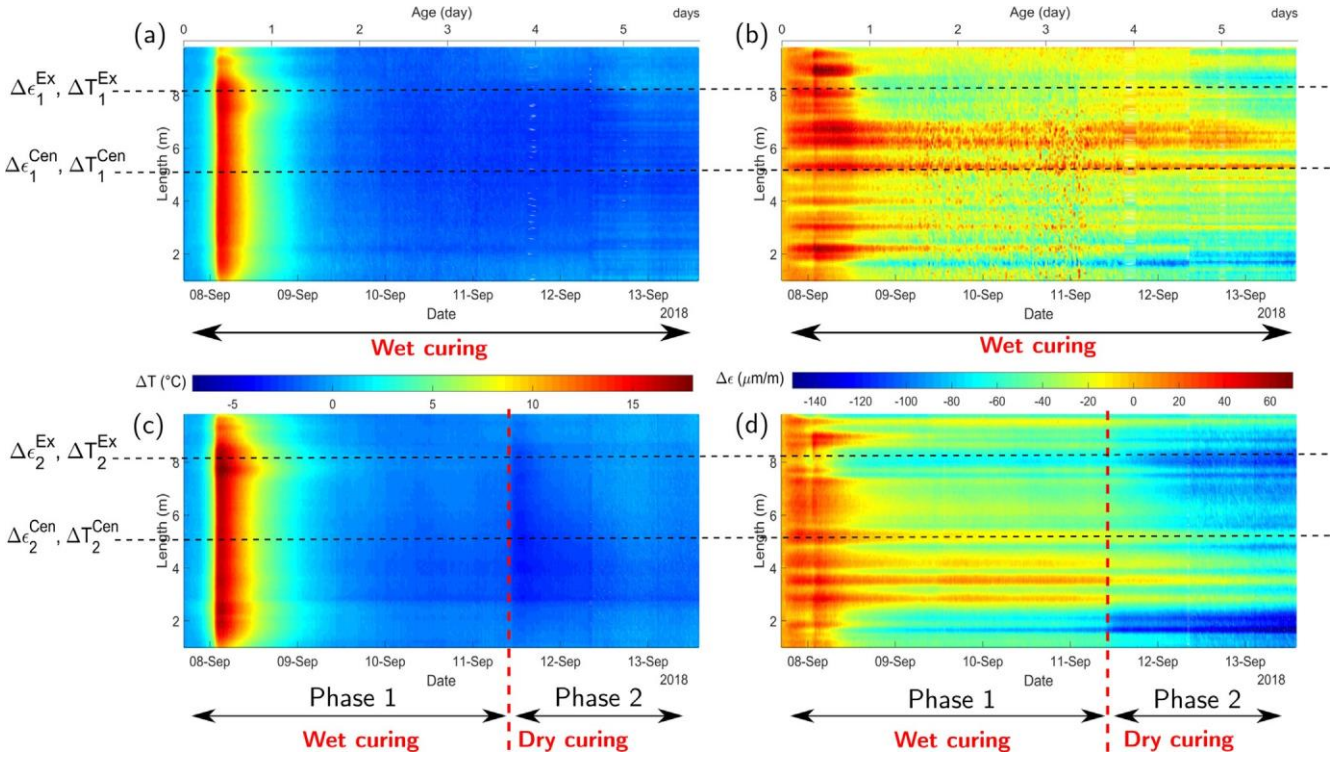

Fig. 9. Temperature and strain mapping along (a,b) slab#1 and (c,d) slab#2.

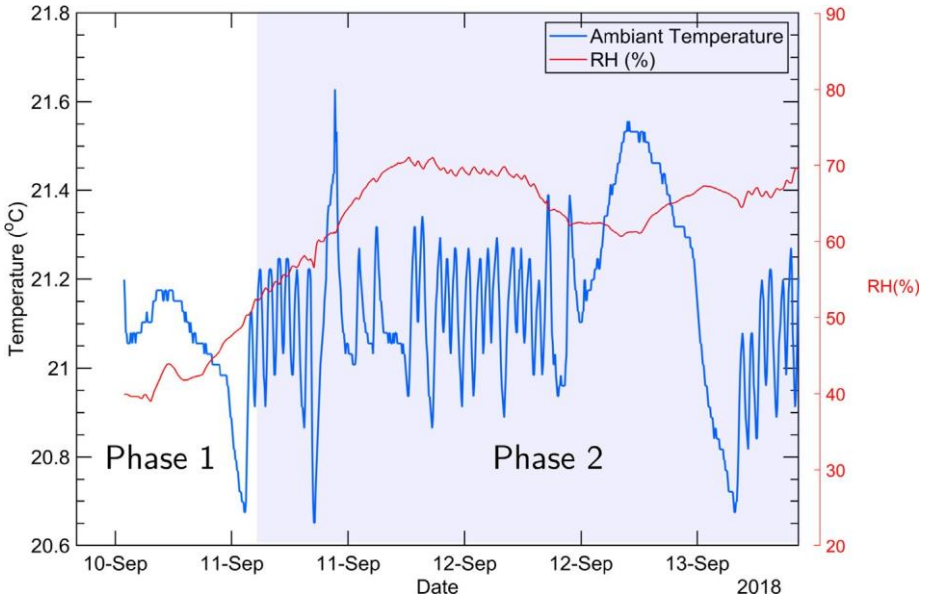

Fig. 10. Temperature and relative humidity readings during the Phases 1 and 2.

After about 4 days of humid curing of the slabs, the shrinkage started to slow down. At this stage, the concrete reached about 70% of its nominal compressive strength (*cf* Table 4). It was thus decided to change the curing conditions of the slab#2. This was done by removing the plastic sheet and thus exposing the concrete surface directly to its surrounding environment (*cf* Fig. 12c). It was observed an immediate effect on the temperature and deformation of the second slab. The slab reacted directly with a drop of temper- ature (*cf* Fig. 11 and a sharp contraction (*cf* Fig. 11b and c). The net shrinkage of the slabs was mainly due to the drying shrinkage which was caused by the water evaporation [45]. The curing conditions slightly affect the temperature evolution, e.g., a drop of about 2 °C of temperature can be observed at the beginning of the Phase 2 due to sudden start of evaporation. The effect can be better visualized at the center of the slab (*cf* Fig. 11c). The process of evaporation (or drying) occurred gradually over the 10 first hours. Fig. 12 shows images of the slab surface during the drying process. The images correspond to the locations 1, 2 and 3 which are indicated in Fig. 11b. The rate of contraction increases at the beginning as the evaporation rate increases. It then becomes more

stable when the slab surface become completely dry (*cf* Fig. 12c). Therefore, by the end of these monitoring phases a significant difference existed between the contraction of both slabs.

4.2. Early-age deformation of the TCC slabs

The data acquisition by OF was stopped on the 6th day in order to put in place the DOFS system for the timber part of the two slabs before being moved on the supports. There was approximately a19 h gap between the end of Phase 2 and the beginning of Phase 3. Due to some technical problems related to the sensors installation, only one of the slabs (slab#1) was equipped with DOFS. The position of the sensors along the height of the timber part is shown in Fig. 6. The slabs were also equipped with traditional displacement sensor to measure the deflection at the mid-span and the slip between the timber and the concrete at the extremities respectively.

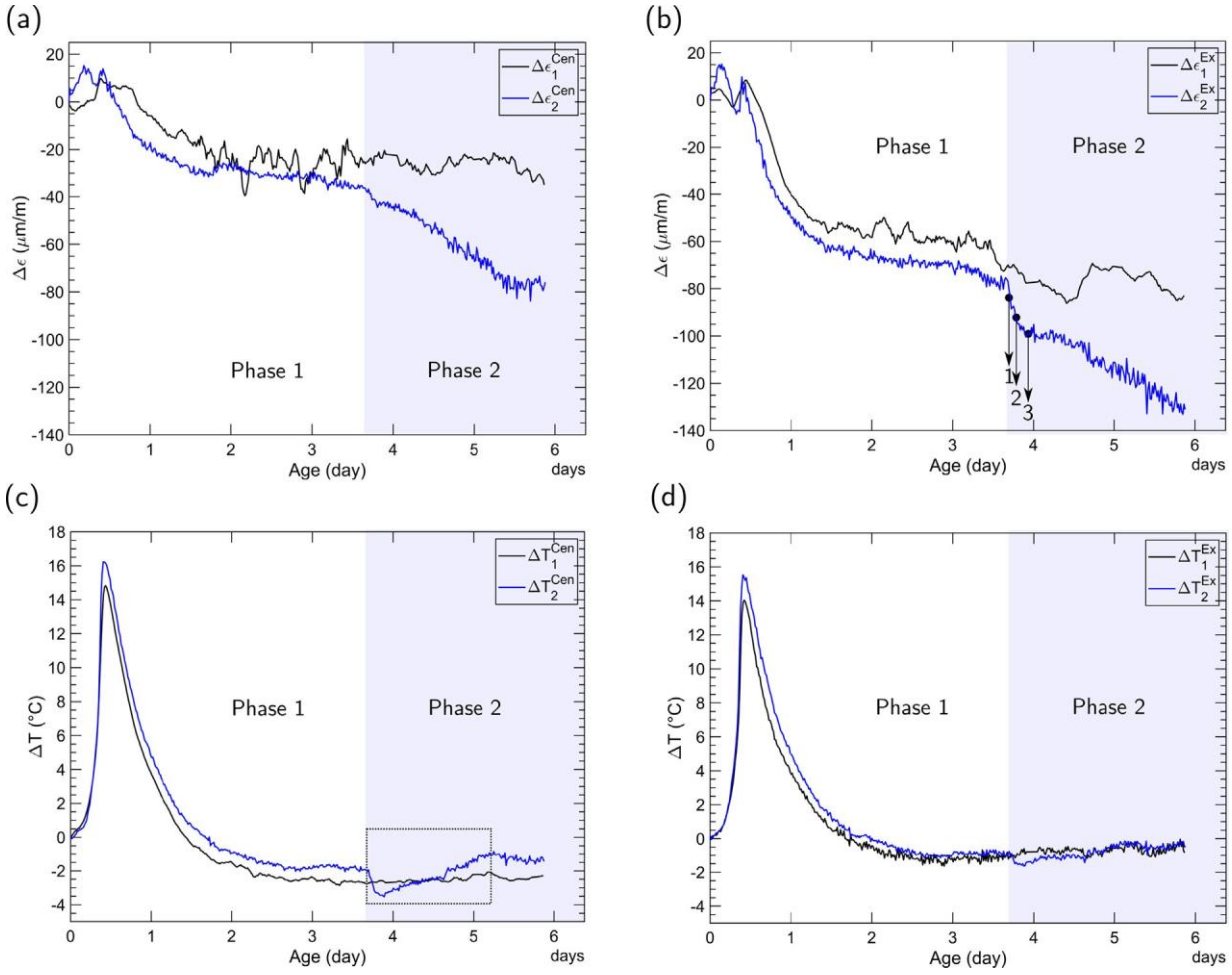

Fig. 11. Temporal evolution of strain and temperature ($\Delta\boldsymbol{\varepsilon}$; ΔT) changes in: (a, c) the center ($\Delta\boldsymbol{\varepsilon}i^{Cen}$; ΔT_i^{Cen}) and (b, c) the extremity ($\Delta\boldsymbol{\varepsilon}i^{Ex}$; ΔT_i^{Ex}) of both slabs.

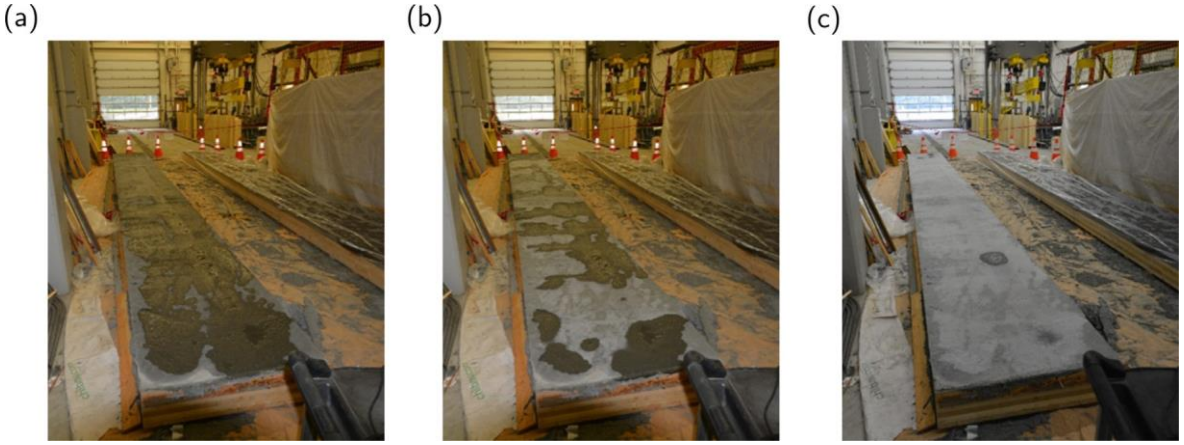

Fig. 12. Drying of the surface of the slab#2 after removal of plastic sheet. Images (a), (b) and (c) correspond respectively to the instants (1), (2) and (3) in the Fig. 11b.

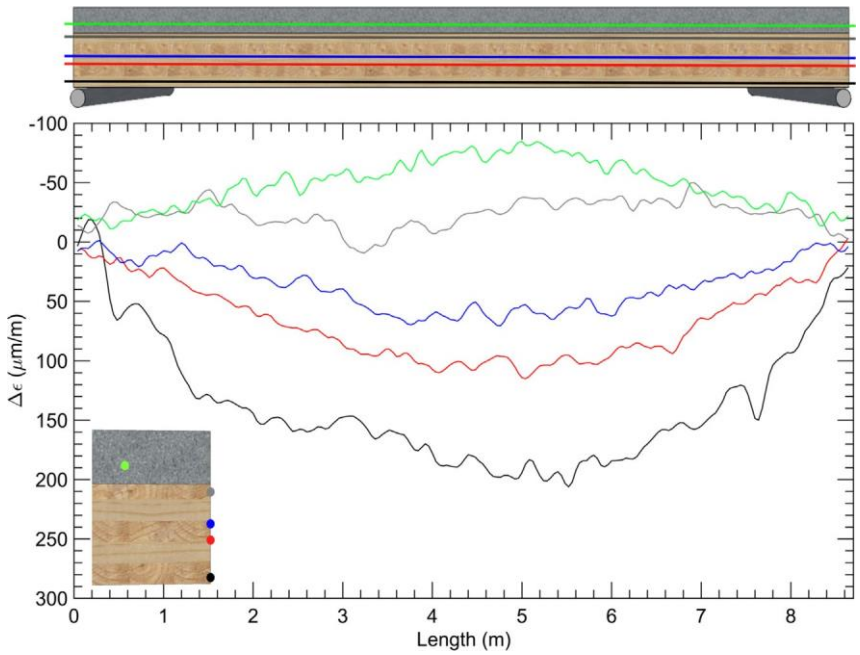

Fig. 13. Initial deflection of the slab#2, measured immediately after the positioning of the slab on 2 supports. Strain along different fiber paths is represented (baseline = slab on the ground). The position of each of the paths is indicated on the bottom-left corner of the figure.

4.2.1. Initial deflection

Following the installation of the slab on the simple supports, it underwent an initial deflection under the effect of its self-weight. Fig. 13 illustrates the axial strain profile along the FO paths installed at different heights of the slab#1. The values of the strain were measured with respect to a reference baseline captured when the slab was still on the ground. The procedure described in Section 4.1.1 was used to align different fiber paths with respect to each other. For the fibers bonded to the timber, the temperature was compen- sated using an external sensor while the temperature inside the concrete was compensated using the fiber placed in the cooper tube that was embedded beforehand inside the concrete (*cf* Fig. 6). Regarding the distribution of the strain, it can be observed that the timber part of the slab was under tension strain while the fiber embedded in the concrete showed compressive strain. This behav- ior is typical for TCC sections, i.e. in TCC slabs subjected to bending, the location of the neutral axis is different from the mid-plane of the timber section. The section can be viewed as under a combination of bending moment and axial tension. The neutral axis in the pre- sent case was located near the upper fiber of the section, suggesting the establishment of a high degree composite action between the timber and the concrete. Another observation is that the strain along the slab length presented some non-uniformities, especially OF placed in the vicinity of the concrete slab. This variation may have been caused by the interaction between the concrete and tim- ber through the connection system.

4.2.2. Time-dependent behavior

Fig. 14a illustrates the evolution of the axial strain in the mid-span-cross section of the slab#1. It is recalled that the values of the strain were measured with respect to a reference baseline captured when the slab was still on the ground. The daily variation of the relative humidity (RH) of the laboratory is also plotted in Fig. 14a. The temperature of the laboratory was controlled at 21°C ± 0.5°C.

From Fig. 14, it can be observed that the short-term behavior of the slab varies significantly over time. First, the strain increased during the 4 first days (from 14-Sep to 19-Sep). After that time, the deflection showed a cyclic tendency, which seemed to be dri- ven by changes in the relative humidity of the laboratory. In fact, the deformation of the slab mirrored, with a delay of few hours, the relative humidity curve of the laboratory. The deformation of the slab increased as the relative humidity increased (humidification of the timber) and decreased when the relative humidity (drying of the timber) decreased. An analysis of the relative deflection of the second slab seems to corroborate these observations (*cf* Fig. 14b). The relative deflection was measured by a displacement sensor. It was reset immediately after the installation of the slab on the support. Therefore, the data do not include the initial elastic deflection (about 8.5 mm).

The fiber embedded in the concrete revealed an initial compressive strain that increased over time. This strain was a combination of several complex mechanisms such as the concrete shrinkage and the creep as well as the interaction with the timber part of the slab through the connection system, which underwent creep deformation. The sudden drop in relative humidity on Sep-19 (*cf* Fig. 14a.) generated an overall contraction of the CLT slab (the slab tends to return to its initial position). This caused the breaking of the fiber inside the concrete. Measurements were interrupted for few hours and then were re-started after the removal of the defective part of the fiber.

4.2.3. Sectional analysis of timber section

Fig. 15 illustrates the evolution of the strain measured by OF in the CLT slab at mid-span at four time points (t_1-t_4), located as indicated in Fig. 14. The times were chosen because they are specifi- cally relevant to understanding the different deformation mechanisms of the timber slab. The vertical dashed line corre- sponds to zero deformation and its intersection with the strain dia- gram corresponds to the position of the neutral axis of the CLT section.

The diagram t_1 (Sep-14, 10:46 am) represents the axial deformation of the section immediately after the positioning of the slab on the supports (elastic deformation of the slab). It can be observed that the strain diagram is linear, revealing that the CLT section remained flat during its deformation. Also, it appeared that most

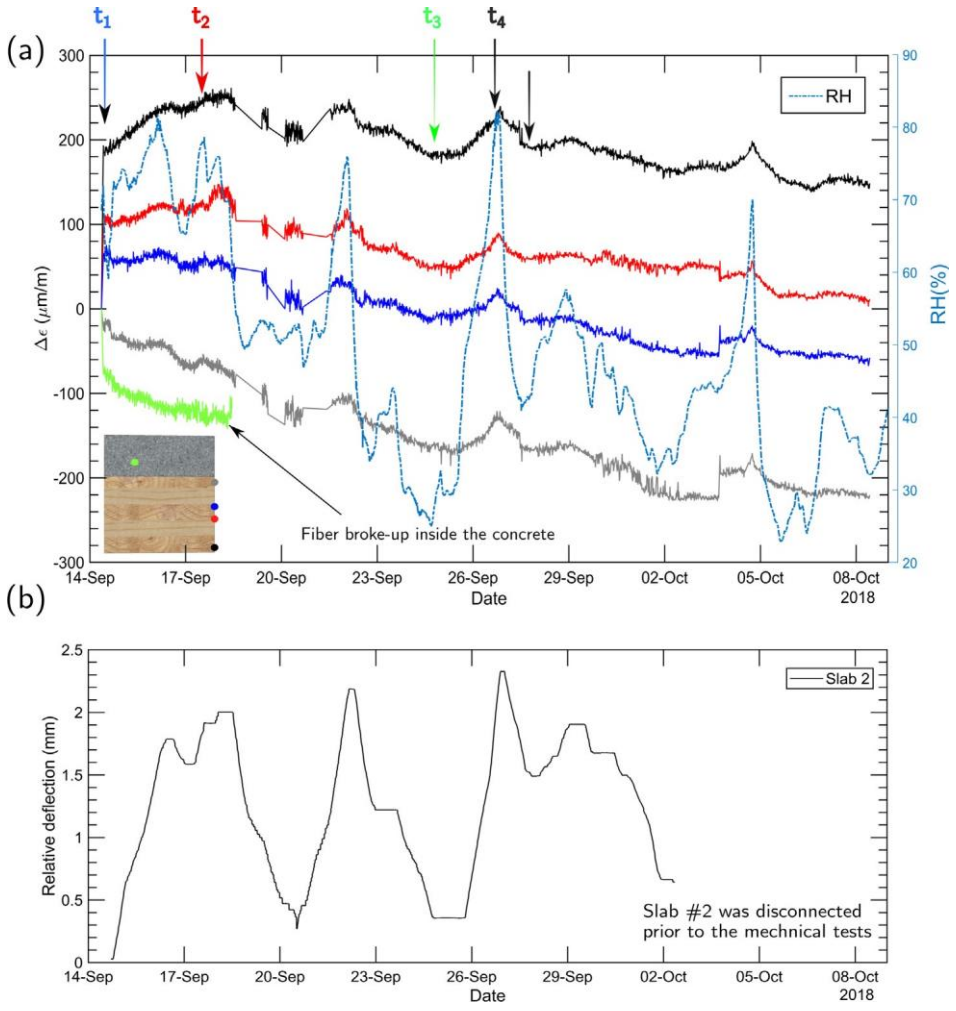

Fig. 14. Temporal evolution of the strain in the middle span section of the slabs. (a) Strain at different heights measured with the DOFS (baseline = slab on the ground). The position of each fiber is indicated on the bottom-left corner of the plot. (b) Temporal evolution of the relative deflection of the slab#2. The relative deflection is measured with respect to a reference considered right after the installation of the slab on the supports.

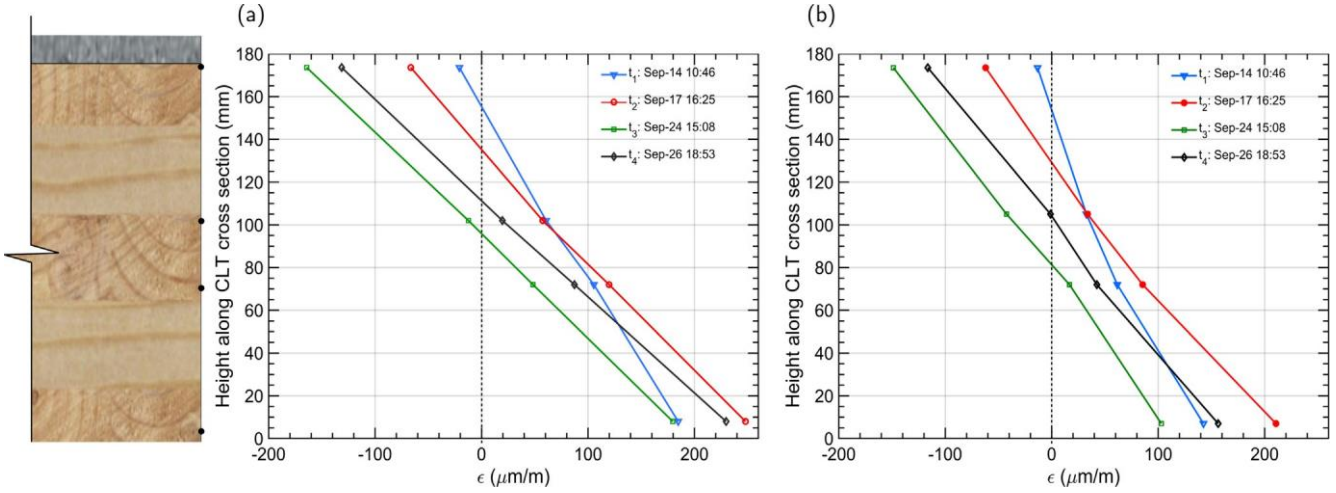

Fig. 15. Strain variation across the TCC section at different times (t_1-t_4), whose location are indicated in Fig. 14a. (a) Mid-span section and (b) quarter-span Section (2 meters from the support).

of the CLT slab was under tension, indicating that the compression is mainly withstood by the concrete slab. Measurements provided by the fiber embedded within the concrete confirm this observation (*cf* Fig. 14a). The time t_2 corresponds to the date (Sep-17, 16h25 pm), i.e. about 77 h from t_1. Comparison of the strain diagram with that of t_1 shows a rotation of the section.

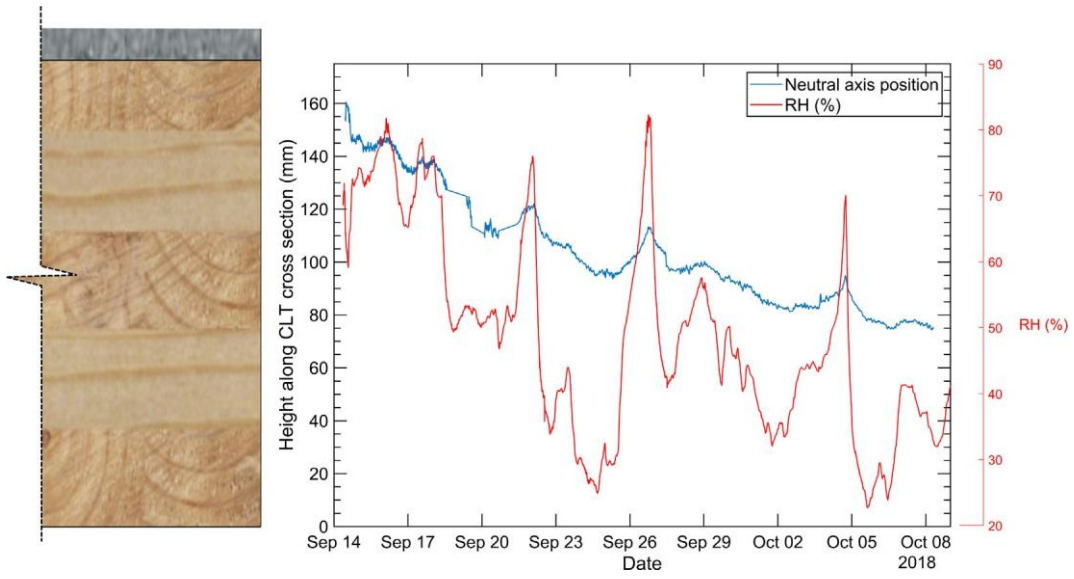

Fig. 16. Temporal evolution of the neutral axis in the timber cross-section.

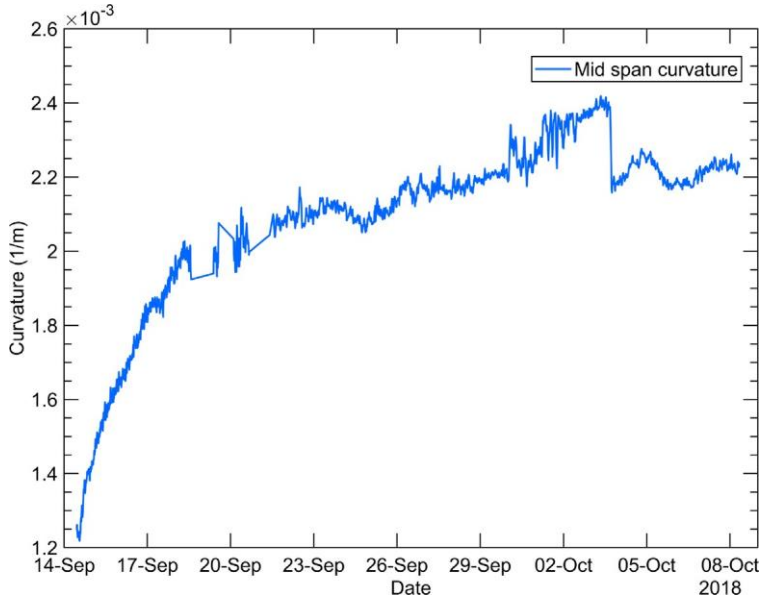

Fig. 17. Mid span CLT curvature evolution over the time.

The tensile and the compressive strains within the section increased respectively, evidencing a creep of the slab. The com- pressive force increased due to concrete shrinkage and the neutral axis of the section moved down, suggesting a slight loss of composite action between the timber and the concrete. It seemed that at this level, the deformation of the slab was mainly driven by the concrete shrinkage and the creep of the concrete and the timber.

The time t_3 (Sep-24 15:08 pm) corresponds to the sudden drop in the relative humidity of the laboratory (*cf* Fig. 14a). By comparing the diagrams t_2 and t_3, it can be observed that they are almost par- allel (they keep the same curvature), indicating a uniform compres- sion of the CLT-section between those two states. The hygroscopic phenomenon of timber can explain this observation [12]. In fact, the moisture content of the timber is directly dependent on the rel- ative humidity of the environment, and its changes induce the swelling/shrinking of the timber. This results in a uniform strain in the CLT cross-section. In contrast, at the time t_4, where the relative humidity reached a peak (81%), the humidification of the timber caused a uniform expansion of the section. In fact, the diagram corresponding to t_4 is a translation of t_3 in the tensile direction.

Using the measured strain values along the CLT section, the evolution of the neutral axis of the CLT slab can be measured along its length over the entire monitoring period. Clearly the DOFS system provide much more information on the structural behavior of TCC slabs than the traditional sensors.

4.2.4. Neutral axis depth and curvature evolution at early-age

In TCC structures, the position of the neutral axis in the timber cross-section is a good indicator of the degree of composite action existing between the timber and the concrete. In fact, when a full-composite action is achieved between both materials, they become rigidly connected without any relative slip between them. In this case, the cross-section of the slab has a single neutral axis and the flexural strains at the timber-concrete interface are identical for both materials. However, in TCC structures, a fully composite

action is not usually achievable, and the slip cannot be prevented. TCC structures exhibit most often a partial composite action. In that instance, the single neutral axis splits, and each one of the layers become characterized by its own neutral axis. As the slip between the layers increases, both neutral axes move farther apart [46]. Hence, the information about the neutral axis position in the timber slab provides useful information about the health of whole TCC slab.

Fig. 16 represents the temporal evolution of the neutral axis of the CLT mid-span section. At the beginning, it can be observed that the neutral axis was positioned near the interface between the timber and the concrete, confirming a robust composite action between them. However, the position of the neutral axis descends rapidly towards the center of the timber section indicating the development of an axial force of traction that is caused by the concrete shrinkage. In fact, as the structure is subjected only to its self-weight, the neutral axis evolution is mainly caused by the time-dependent behavior of the slab components. The fact that the components are connected implies that the change in the behavior of one component creates strain/stress in the other [47].

Another relevant quantity such as the curvature at the CLT mid-span section is reported in Fig. 17. This quantity can give interesting information on the slab behavior as it directly proportional to the moment supported by the timber member. The curvature of CLT section was determined by fitting a linear function over the strain diagrams showed in Fig. 15.

It can be observed from Fig. 17 that the curvature increased rapidly in the first 3 days, due to the creep of the TCC slab as well as the shrinkage of the concrete. After this period the curvature stabilized. It also can be seen that the curvature was not affected by the relative humidity of the laboratory, mainly because the swelling/shrinking of the timber is uniform in CLT cross-section.

5. Conclusions and perspectives

This study is the first attempt to implement Brillouin-based scattering DOFS system for monitoring the early-age behavior of two TCC slabs. The monitoring started from the concrete pouring and continued throughout the first 30 days of their pre-service life. The main concluding remarks can be summarized as follows:

- The OF sensors were successively embedded within the fresh concrete slab and allowed continuous measurement of the strain/temperature along its length. They captured with precision the early-age mechanisms related to the curing process of concrete;
- The multiplexing capabilities of DOFS system offered the possibilities to measure the strains at several heights of the timber section using a single sensor. The measurement allowed the full characterization of the strain evolution along the CLT slab over the entire monitoring period;
- The changes of the composite action between timber and concrete was monitored using indicators such as the neutral axis position and the curvature evolution within the CLT slab. It was experimentally shown that mechanisms such as creep and the thermos-hygrometric variations of the environment generate considerable structural changes in the composite elements even before their entry into service. The observations reported in this paper confirm the necessity for the designers and experts to take into consideration such effects during the design process of TCC structures.

Finally, the results presented in this study demonstrate that DOFS system is an interesting tool for monitoring civil engineering structures in general and TCC structures in particularly. However, the installation of OF is relatively difficult to undertake and requires a greater degree of precision and care. Development must be undertaken to provide low-cost protective encapsulation or packaging for the bare fiber. These protections must also guarantee an optimal transfer of the strain from the structure to the fiber.

The outcomes of this study can be applied to future projects, in order to optimize the formwork design of TCC structures and better consider the effect of early-age prestress on the long-term behavior [48,10].

Conflict of interest

The authors declare that there is no conflict of interest regard- ing the publication of this article.

Acknowledgements

The authors gratefully acknowledge the Canada Foundation for Innovation (FCI grant reference number 36933) for purchasing the DOFS system used in this study. The authors want also to thank the Natural Sciences and Engineering Research Council of Canada (CRSNG-CRD) for providing the salary of the corresponding author.

References

[1] Michael H. Ramage, Henry Burridge, Marta Busse-Wicher, George Fereday, Thomas Reynolds, Darshil U. Shah, Guanglu Wu, Li Yu, Patrick Fleming, Danielle Densley-Tingley, et al., The use of timber in construction: the wood from the trees, Renew. Sustain. Energy Rev. 68 (2017) 333–359.
[2] Samuel C. Auclair, Luca Sorelli, Alexander Salenikovich, Simplified nonlinear model for timber-concrete composite beams, Int. J. Mech. Sci. 117 (2016) 30–42.
[3] Ario Ceccotti, Composite concrete-timber structures, Prog. Struct. Mat. Eng. 4 (3) (2002) 264–275.
[4] Peggi Clouston, Leander A. Bathon, Alexander Schreyer, Shear and bending performance of a novel wood–concrete composite system, J. Struct. Eng. 131 (9) (2005) 1404–1412.
[5] Sharon Zingg, Guillaume Habert, Tobias Lämmlein, Pietro Lura, Emmanuel Denarié, and Amir Hajiesmaeili. Environmental assessment of radical innovation in concrete structures. Expanding Boundaries: Systems Thinking for the Built Environment, 2016..
[6] David Yeoh, Massimo Fragiacomo, Mary De Franceschi, Koh Heng Boon, State of the art on timber-concrete composite structures: literature review, J. Struct. Eng. 137 (10) (2011) 1085–1095.
[7] Massimo Fragiacomo, Amedeo Gregori, Junqing Xue, Cristoforo Demartino, Matteo Toso, Timber-concrete composite bridges: three case studies, J. Traffic Transp. Eng. (English Edition) (2018).
[8] Dejian Shen, Xingzuo Liu, Qiyao Li, Lei Sun, Wenting Wang, Early-age behavior and cracking resistance of high-strength concrete reinforced with dramix 3D steel fiber, Constr. Build. Mater. 196 (2019) 307–316.
[9] Dejian Shen, Ci Liu, Chengcai Li, Xiaoguang Zhao, Guoqing Jiang, Influence of barchip fiber length on early-age behavior and cracking resistance of concrete internally cured with super absorbent polymers, Constr. Build. Mater. 214 (2019) 219–231.
[10] Massimo Fragiacomo, Long-term behavior of timber-concrete composite beams. II: Numerical analysis and simplified evaluation, J. Struct. Eng. 132 (1) (2006) 23–33.
[11] Kanhchana Kong, Emmanuel Ferrier, Laurent Michel, Amen Agbossou, Experimental and analytical study of the mechanical behavior of heterogeneous glulam-UHPFRC beams assembled by bonding: short- and long-term investigations, Constr. Build. Mater. 100 (2015) 136–148.
[12] Claude Feldman, Pambou Nziengui, Rostand Moutou Pitti, Eric Fournely, Joseph Gril, Gaël Godi, Samuel Ikogou, Notched-beam creep of Douglas fir and white fir in outdoor conditions: experimental study, Constr. Build. Mater. 196 (2019) 659–671.
[13] Massimo Fragiacomo, Jörg Schänzlin, Proposal to account for concrete shrinkage and environmental strains in design of timber-concrete composite beams, J. Struct. Eng. 139 (1) (2012) 162–167.
[14] Robert Le Roy, Adeline Confrère, Louisa Loulou, Sabine Caré, and Boumediene Nedjar. Auto contraintes dues au retrait endogène dans une structure mixte bois-béton assemblée par collage ''frais sur frais. In 31èmes Rencontres de l'AUGC, ENS Cachan, 29 au 31 mai 2013, pages 11–p, 2013..
[15] António Barrias, Joan R Casas, Sergi Villalba, A review of distributed optical fiber sensors for civil engineering applications, Sensors 16 (5) (2016) 748.
[16] António Barrias, Joan R Casas, Sergi Villalba, Embedded distributed optical fiber sensors in reinforced concrete structures-a case study, Sensors 18 (4) (2018) 980.

[17] Weiwei Lin, Liam J Butler, Mohammed ZEB Elshafie, Campbell R Middleton, Performance assessment of a newly constructed skewed half-through railway bridge using integrated sensing, J. Bridge Eng. 24 (1) (2018) 04018107.
[18] António Barrias, Gerardo Rodriguez, Joan R Casas, Sergi Villalba, Application of distributed optical fiber sensors for the health monitoring of two real structures in Barcelona, Struct. Infrastruct. Eng. 14 (7) (2018) 967–985.
[19] Du. Yang, Yizheng Chen, Yiyang Zhuang, Chen Zhu, Rex E Gerald, Jie Huang, A uniform strain transfer scheme for accurate distributed optical fiber strain measurements in civil structures, Inventions 3 (2) (2018) 30.
[20] Aghiad Khadour, Julien Waeytens, Monitoring of concrete structures with optical fiber sensors, in: Eco-Efficient Repair and Rehabilitation of Concrete Infrastructures, Elsevier, 2018, pp. 97–121.
[21] Liam J Butler, Niamh Gibbons, Ping He, Campbell Middleton, Mohammed Z.E.B. Elshafie, Evaluating the early-age behaviour of full-scale prestressed concrete beams using distributed and discrete fibre optic sensors, Constr. Build. Mater. 126 (2016) 894–912.
[22] Liam J. Butler, Weiwei Lin, Xu Jinlong, Niamh Gibbons, Mohammed Z.E.B. Elshafie, Campbell R. Middleton, Monitoring, modeling, and assessment of a self-sensing railway bridge during construction, J. Bridge Eng. 23 (10) (2018) 04018076.
[23] Maheshwar Ghimire, Chuji Wang, Kenneth Dixon, Michael Serrato, In situ monitoring of prestressed concrete using embedded fiber loop ringdown strain sensor, Measurement 124 (2018) 224–232.
[24] Branko Glisic, Daniele Inaudi, Structural monitoring of hybrid specimens at early age using fibre optic sensors, in: Proceedings of the 55th Rilem Annual Week, Symposium on connections between Steel and Concrete, Stuttgart, Germany, 2001, pp. 9–12..
[25] Allan C.L. Wong, Paul A. Childs, William Terry, Nadarajah Gowripalan, Gang-Ding Peng, Experimental investigation of drying shrinkage and creep of concrete using fibre-optic sensors, Adv. Struct. Eng. 10 (3) (2007) 219–228.
[26] Ying-Wei Yun, Il-Young Jang, Research on early age deformation of high performance concrete by fiber Bragg grating sensor, KSCE J. Civ. Eng. 12 (5) (2008) 323.
[27] Ying-Wei Yun, Il-Young Jang, Wan-Wen Wang, Early-age autogenous shrinkage of high-performance concrete columns by embedded Fiber Bragg-Grating sensor, KSCE J. Civ. Eng. 16 (6) (2012) 967–973.
[28] Huafu Pei, Qing Yang, Zongjin Li, Early-age performance investigations of magnesium phosphate cement by using fiber Bragg grating, Constr. Build. Mater. 120 (2016) 147–149.
[29] Giovanna Palumbo, Agostino Iadicicco, Francesco Messina, Claudio Ferone, Stefania Campopiano, Raffaele Cioffi, Francesco Colangelo, Characterization of early age curing and shrinkage of Metakaolin-based inorganic binders with different rheological behavior by fiber Bragg grating sensors, Materials (Basel) 11 (1) (2017).
[30] Chen Hou, Wancheng Zhu, Baoxu Yan, Kai Guan, Du. Jiafa, Influence of binder content on temperature and internal strain evolution of early age cemented tailings backfill, Constr. Build. Mater. 189 (2018) 585–593.
[31] Ahmed Loukili, David Chopin, Abdelhafid Khelidj, Jean-Yves Le Touzo, A new approach to determine autogenous shrinkage of mortar at an early age considering temperature history, Cem. Concr. Res. 30 (6) (2000) 915–922.
[32] Dong Luo, Zubaidah Ismail, Zainah Ibrahim, Added advantages in using a fiber bragg grating sensor in the determination of early age setting time for cement pastes, Measurement 46 (10) (2013) 4313–4320.
[33] Carlos Augusto Galindez-Jamioy, Jose M. Lopez-Higuera, Brillouin distributed fiber sensors: an overview and applications, J. Sens. 2012 (2012).
[34] Jean-Marie Henault, Gautier Moreau, Sylvain Blairon, Jean Salin, Jean-Robert Courivaud, Frédéric Taillade, Erick Merliot, Jean-Philippe Dubois, Johan Bertrand, Stéphane Buschaert, et al., Truly distributed optical fiber sensors for structural health monitoring: from the telecommunication optical fiber drawling tower to water leakage detection in dikes and concrete structure strain monitoring, Adv. Civil Eng. 2010 (2010).
[35] Branko Glisic, Daniele Inaudi, Fibre Optic Methods for Structural Health Monitoring, Chapter Fibre-Optic Deformation Sensors: Applicability and Interpretation of Measurements, John Wiley & Sons, 2008, pp. 41–81.
[36] Dongsheng Li, Liang Ren, Hongnan Li, Mechanical property and strain transferring mechanism in optical fiber sensors, in: In Fiber Optic Sensors, InTech, 2012.
[37] G. Pereira, C. Frias, H. Faria, Orlando Frazão, A.T. Marques, On the improvement of strain measurements with FBG sensors embedded in unidirectional composites, Polym. Testing 32 (1) (2013) 99–105.
[38] T. Landolsi, L. Zou, O. Sezerman, Utility applications of fiber-optic distributed strain and temperature sensors. Technical report, 2015..
[39] ASTM A1064/A1064M-18a, Standard Specification for Carbon-Steel Wire and Welded Wire Reinforcement, Plain and Deformed, for Concrete1. Standard, ASTM International, West Conshohocken, 2018.
[40] Serge Lamothe, Luca Sorelli, Pierre Blanchet, Philippe Galimard, Development of a rigid-ductile notch connector for timber composite structures with cross laminated and glued laminated timber. Submitted..
[41] ACI Committee 308, 308R-16 Guide to External Curing of Concrete. Standard, 2016..
[42] Allan CL Wong, Paul A Childs, Richard Berndt, Tony Macken, Gang-Ding Peng, Nadarajah Gowripalan, Simultaneous measurement of shrinkage and temperature of reactive powder concrete at early-age using fibre Bragg grating sensors, Cem. Concr. Compos. 29 (6) (2007) 490–497.
[43] Xiaotian Zou, Alice Chao, Ye Tian, Wu. Nan, Hongtao Zhang, Yu Tzu-Yang, Xingwei Wang, An experimental study on the concrete hydration process using fabry-perot fiber optic temperature sensors, Measurement 45 (5) (2012) 1077–1082.
[44] Robert F Ytterberg, Control of shrinkage and curling in slabs on grade, Concr. Constr. (1992) 825–831.
[45] Hani Nassif, Nakin Suksawang, Maqbool Mohammed, Effect of curing methods on early-age and drying shrinkage of high-performance concrete, Transp. Res. Rec.: J. Transp. Res. Board 48–58 (1834) (2003).
[46] Elzbieta Lukaszewska, Development of prefabricated timber-concrete composite floors (Ph.D. thesis), Luleå tekniska universitet, 2009.
[47] Thomas Tannert, B. Endacott, M. Brunner, T. Vallée, Long-term performance of adhesively bonded timber-concrete composites, Int. J. Adhes. Adhes. 72 (2017) 51–61.
[48] Ario Ceccotti, Massimo Fragiacomo, Saverio Giordano, Long-term and collapse tests on a timber-concrete composite beam with glued-in connection, Mater. Struct. 40 (1) (2006) 15–25.